Detection of intrinsic stress in cubic boron nitride films by x-ray absorption near-edge structure: Stress relaxation mechanisms by simultaneous ion implantation during growth

R. Gago,[1,*] B. Abendroth,[2] J. I. Cerdá,[3] I. Jiménez,[3] and W. Möller[2]
[1]*Centro de Micro-Análisis de Materiales and Departamento de Física Aplicada, Universidad Autónoma de Madrid, E-28049 Madrid, Spain*
[2]*Institute of Ion Beam Physics and Materials Research, Forschungszentrum Dresden-Rossendorf, PF-510119, D-01314 Dresden, Germany*
[3]*Instituto de Ciencia de Materiales de Madrid, Consejo Superior de Investigaciones Científicas, E-28049 Madrid, Spain*
(Received 30 July 2007; revised manuscript received 3 October 2007; published 19 November 2007)

The bonding structure of cubic boron nitride (*c*BN) films with different levels of intrinsic stress (1–10 GPa) has been studied from the *K*-shell x-ray absorption near-edge structure (XANES). The stress level was tuned by the damage induced from simultaneous medium-energy ion implantation (1–10 keV) during growth. The films show a dominant sp^3 arrangement for damage values below a certain threshold, with an appreciable sp^3 to sp^2 transformation taking place above this limit. Interestingly, the degree of stress in sp^3 structures is reflected in the B 1*s* spectral line shape, which progressively converges to that of stress-free *c*BN powder for increasing ion damage. These results indicate that stress buildup and release occur at a microscopic level. The changes in the spectral line shape are correlated with modifications in the electronic structure due to the presence of intrinsic stress and bond distortion within the cubic network, as predicted by density functional theory calculations. Our findings reveal the potential of XANES spectroscopy to detect stress in disordered BN systems.

DOI: 10.1103/PhysRevB.76.174111 PACS number(s): 61.10.Ht, 61.82.Rx, 61.80.Jh, 71.15.Mb

I. INTRODUCTION

Cubic boron nitride (*c*BN) is the second hardest material after diamond. Superior to diamond in some aspects, it does not react with ferrous materials and is resistant to oxidation up to 1300 °C.[1] Therefore, it is a very promising material for hard coatings. In order to grow *c*BN in thin film form, a certain amount of ion bombardment is required to enable the nucleation and subsequent growth of the *c*BN layer. However, ion bombardment additionally induces an undesirable high intrinsic compressive stress (up to −20 GPa) in the growing layer.[2–4] As a consequence, the films delaminate when their thickness exceeds a critical value of a few hundreds of nanometers.

Several ways to reduce the intrinsic stress *c*BN have been reported.[5] Among them, a promising option is the use of medium-energy ion implantation after deposition.[5,6] Based on this, a combination of film growth and *in situ* ion implantation was proposed to attain thick *c*BN films.[5] Under this approach, relatively thick films (~1.3 μm) were successfully produced by a complex process of sequential sputter cleaning, growth, implantation, and further annealing.[7] A more simple alternative can be achieved by using simultaneous ion irradiation during growth at energies between a few and a few tens of keV. The latter proposal for *in situ* stress release has been successfully implemented in ion beam assisted deposition[8] and magnetron sputtering (MS)[9] growth facilities.

Despite the successful stress release upon ion implantation, the detailed mechanisms involved in the process remains unclear. Experimentally, it has been observed that the amount of stress release scales with the ion damage induced from the medium-energy bombardment, as quantified by the average number of displacements per atom (dpa).[8,9] The relaxation process without detrimental *c*BN transformation into hexagonal BN (*h*BN) takes place for damage values below a certain threshold of ~1 dpa.[9] For values above this threshold, the stress saturates at ~1–2 GPa and further increase in the damage only results in a larger *h*BN content.

In order to gain information about the stress release mechanisms, stress measurement should be performed at a microscopic level. However, this is difficult to attain in BN systems for several reasons. First, stress values obtained by substrate bending cannot resolve between contributions arising from intrinsic and extrinsic (film/substrate interface, layer structure, grain boundaries, etc.) sources. Second, the poor crystallinity of the samples (typically grain size in the nanometer range) and the low scattering cross section from low-Z elements make a detailed analysis by x-ray diffraction (XRD) tedious and difficult. The latter may be partially overcome using the brightness of synchrotron radiation.[10] Regarding other characterization techniques, stress and strain have also been related theoretically[11] and experimentally[12] with the in-plane transversal optical phonon energy in the IR spectra. However, this indirect method does not give a univocal dependence with the stress value.[13]

X-ray absorption near-edge structure (XANES) can be used to elucidate the chemical bonding and electronic structure in complex systems.[14] XANES spectroscopy measures optical transitions from core levels to unoccupied states being, due to its local character, well suited for amorphous or nanocrystalline structures. This analysis is even more interesting in BN materials since XANES is very sensitive to different BN allotropes.[15] Therefore, it can provide further hints about the stress release mechanisms at a microscopic level by discerning between the phase transformation and atomic rearrangement occurring at the sample surface. In addition, we can explore the correlation between stress and spectral features, as already reported for other systems.[16]

In the case of simultaneous medium-energy implantation, XRD with synchrotron radiation has shown that the stress release below 1 dpa occurs effectively within the *c*BN grains, as confirmed by the reduction of biaxial strain.[17] However, effects from grain boundaries and amorphous sp^2-sp^3 phases, not detectable by XRD, may also contribute to the stress release. In the present work, we address the bonding structure by XANES of *c*BN films grown under simultaneous medium energy with different ion damage values (<1.2 dpa). The B 1*s* XANES signal shows that the cubic structure is maintained in the near surface in the damage regime below ~1 dpa. Furthermore, while showing a dominant sp^3 character, the B 1*s* line shape is deformed compared to reference *c*BN samples, providing a metric of the bond distortion that scales with the macroscopic stress level. Our conclusions are corroborated by density functional theory (DFT) based electronic structure calculations for bulk *c*BN under strain.

II. EXPERIMENTAL DETAILS

*c*BN films were grown by unbalanced rf-MS from an *h*BN target in Ar/N_2 atmosphere. The growth facility and procedure are described in detail elsewhere.[9] The *in situ* stress relaxation during growth was induced from medium-energy ion implantation by inserting high-voltage (HV) negative pulses (1–10 kV) in the low-voltage (–150 V) substrate bias, the latter needed for the nucleation and subsequent growth of the *c*BN phase. The evolution of film growth and instantaneous stress were monitored *in situ* and in *real time* via a combination of spectroscopic ellipsometry and substrate curvature measurements.[18] For this purpose, the bending of the substrate was followed from the deflection of a laser beam on a cantilever substrate. The overall film thickness was limited to ~100 nm to prevent eventual detachment from the substrate after deposition.

The induced damage from the medium-energy ions was quantified by the number of dpa derived from the ion current density, the HV pulse amplitude, and its duty cycle.[9,19] In this computation, the damage induced by the low-energy ions is not considered for two reasons. First, the same conditions apply to all the films processed, and second, the stress level seems to be "universally" determined by the higher of the energies involved in the deposition.[20] The corresponding preparation parameters, calculated damage, and resulting stress values for the selected set of samples considered in this work are summarized in Table I. The quoted damage values correspond to the average value along the whole film thickness.

The XANES measurements were performed in the synchrotron facility BESSY-II (Berlin, Germany) at the PM4 beamline with the SURICAT end station. The data were acquired in the total electron yield mode (TEY) by recording the current drained to ground from the sample. The sample signal was normalized to the signal recorded simultaneously from a gold covered grid located upstream the x-ray path. In this work, we focus our study on the B 1*s* edge since it contains sharper features than the N 1*s* counterpart[15] and, hence, more information can be extracted.

TABLE I. Growth parameters and *in situ* measured stress of *c*BN films produced under simultaneous medium-energy ion implantation during MS as a function of the ion induced damage (in displacements per atom, dpa). The stress measurements are derived from the bending method (following the deflection of a laser beam on a cantilever substrate).

Damage (dpa)	Low bias voltage (V)	High bias voltage (kV)	Duty cycle (%)	Stress (GPa)
0.0	−150	0		−10.7±0.1
0.6	−150	−8	0.3	−2.0±0.1
0.7	−150	−4	0.6	−1.7±0.1
1.2	−150	−8	0.6	−1.6±0.1

III. THEORETICAL DETAILS

Although XANES spectroscopy is a powerful technique to assess the bonding structure of disordered materials, it presents a complex framework for accurate simulations.[21] First, the measured signal involves the description of the optical transition from a core electron to the unoccupied electronic states, thus requiring an accurate description of the system's ground state plus the inclusion of core-hole effects.[22] Second, the emitted electrons suffer multiple scattering processes before exiting the sample,[23] implying a further nontrivial dependence on energy.

Given the complex atomic network of our samples, lacking any long range order and comprising multiple bonding environments, accurate XANES spectra simulations become unattainable here. Instead, we will focus on changes in the electronic structure as extracted from the unoccupied projected density of states (PDOS) onto the selected element,[24] the boron (B) atoms in our case. Although we do not expect that such a simplified approach will reproduce every detail of the XANES signal, it should reveal the correlation between the PDOS and the observed XANES trends.[24]

Accordingly, we have studied the evolution of the B PDOS starting from an ideal *c*BN bulk unit cell with lattice parameter of 0.3615 nm. Following the experimentally observed strain,[17] we allowed for positive and negative stretching of the equilibrium *c*BN structure along the {111} direction, as illustrated in Fig. 1. For this purpose, the periodicity along the {111} direction, *c*, is varied around the equilibrium value of ~0.21 nm in the $0.20\ \text{nm} < c < 0.35\ \text{nm}$ range. All the theoretical calculations have been performed with the pseudopotential[25] DFT based SIESTA code,[26] considering both the generalized gradient approximation (GGA)[27] and local density approximation[28] to the exchange correlation. However, both approximations yielded the same qualitative conclusions, and we will only present hereafter results derived from the GGA approach. Since SIESTA employs linear combinations of atomic orbitals (AOs) as basis sets, it allows the calculation of the PDOS onto the B atoms in a natural way. In order to accurately describe the valence states, we employed a double zeta polarized basis set, both for N and B, while the rest of the parameters entering the

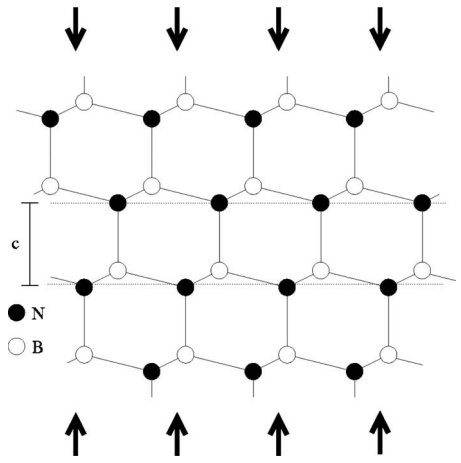

FIG. 1. Side view of the *c*BN system studied in this work. The arrows indicate the stress applied along the {111} direction. In the simulations, we modeled this uniaxial stress by varying the *c* parameter while fixing the in-plane lattice constant *a*. Note that as *c* is increased, the structures tend toward the layered configuration of *h*BN, i.e., the sp^3 hybridization progressively transforms into sp^2.

calculation (*k* sampling, AO localization, and the accuracy in the real space grid integrals) were set to well converged values.

IV. RESULTS AND DISCUSSION

A. Bonding structure by x-ray absorption near-edge structure

Figure 2 shows in the upper curve the B 1*s* XANES spectrum of a *c*BN sample produced by MS without HV pulses. This growth condition leads to high level of stress (~10 GPa), as measured by the substrate bending method.[9] Reference spectra from BN powders with cubic (*c*BN) and wurtzite (*w*BN) structures are shown as signatures for stress-free sp^3 allotropes. The *w*BN phase presents the same first coordination shell as in *c*BN but with a hexagonal structure due to the *ABAB* stacking sequence of atomic layers along the {0001} direction instead of the *ABCABC* stacking in *c*BN along its {111} direction.[29] Also, the spectrum from *h*BN is shown as a reference signal for sp^2 hybrids. In the case of *h*BN, the spectrum shows a prominent peak at 192 eV corresponding to the π^* excitonic resonance of π bonds in planar sp^2 structures and, hence, should be absent in sp^3 materials.[15] The sp^2 arrangement is also reflected in the absorption spectrum with the presence of two onsets related to transitions from 1*s* levels to π^* and σ^* states above 192 and around 197 eV, respectively (see the magnified curve for the *h*BN reference). Note the high intensity of the π^* resonance peak with respect to the σ^* edge for the reference sp^2 material. In the case of the *c*BN and *w*BN sp^3 phases, the spectra show a single edge corresponding to $1s \rightarrow \sigma^*$ transitions around 194 and 195 eV, respectively. Despite having the same first coordination shell for *c*BN and *w*BN sp^3 phases, the onset and line shape of the σ^* states differ for each allotrope and, therefore, are direct fingerprints for each bonding environment (extended to at least two coordination shells). In the *w*BN phase, the dominant feature appears as a broad peak at ~195.5 eV, labeled as A in Fig. 2, whereas in *c*BN, the highest intensity, labeled as B, is located at ~198 eV.

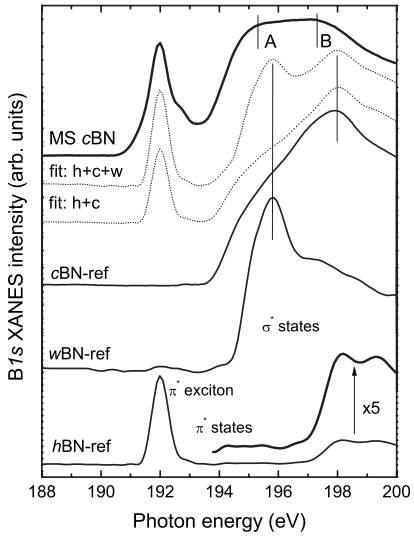

FIG. 2. B 1*s* XANES spectrum (top curve) from a *c*BN coating grown by magnetron sputtering (MS) with high intrinsic stress (−10 GPa). The reference spectra from *h*BN, *c*BN, and *w*BN powders (bottom curves) are shown as the fingerprint of sp^2 and sp^3 structures. The spectrum of *w*BN has been taken from Ref. 15. The dotted curves are obtained as a linear combination of the hexagonal (*h*), cubic (*c*), and wurzite (*w*) references (with sp^2 content of ~15%).

The spectrum from the MS *c*BN sample has a dominant σ^* band starting at 194 eV, as in *c*BN, and a minor π^* band extending below this value. The main σ^* band indicates the dominance of sp^3 hybrids in this material and seems to be composed of both features A and B discussed above with almost equal intensity, although shifted by about 0.5 eV to lower energies. This observation suggests the possibility of a mixture of *c*BN and *w*BN phases. The lower contribution of π^* states is probably due to sp^2 hybrids located at grain boundaries and/or as a terminating surface layer.

An estimate of the sp^3/sp^2 ratio for the MS *c*BN sample can be obtained by fitting the spectrum with a linear combination of the *h*BN and *c*BN reference spectra.[30] The best fit under this approach is shown in the dotted curve of Fig. 2 (fit: $h+c$) and gives an sp^3 fraction of ~85%. Although the sp^3 value is reasonable, the line shape fitting is not satisfactory because the intensity of the σ^* edge around 195 eV (feature A) appears too low as compared to the experimental data. Due to the pronounced intensity in this spectral region from *w*BN (see Fig. 2), the possible contribution of this bonding environment has also been checked to explain the line shape of MS *c*BN. However, the introduction of this third component leads to the same sp^2 content but the spectral line shape is again poorly fitted (see fit: $h+c+w$ in Fig. 2). Further, previous XRD analysis of these samples has only detected the contribution from *h*BN and *c*BN phases.[17] Hence, an alternative explanation is addressed in terms of bond distortion in the cubic structure induced by the high level of intrinsic stress. In particular, XRD analysis has

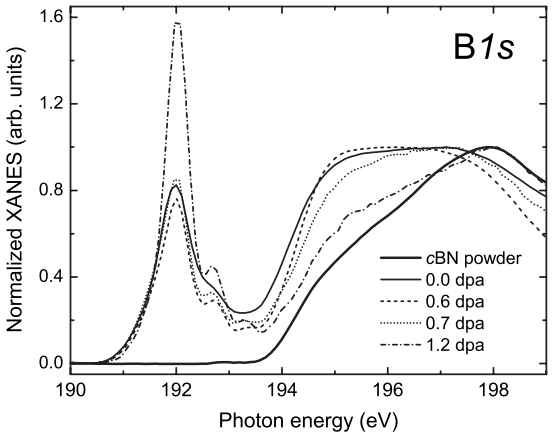

FIG. 3. B 1*s* XANES spectra for BN samples produced with different ion induced damage from medium-energy bombardment during growth, together with a stress-free reference from polycrystalline *c*BN powder. The spectrum for the sample grown with 0 dpa is the same as the top curve displayed in Fig. 2.

shown that the films are under biaxial compressive stress, which results in a reduced and extended *in-plane* and *out-of-plane* lattice parameters, respectively.[17] This fact should be considered in addition to the effect of an eventual bond-length distribution coming from the disordered nature of the samples and the presence of stress. It has been shown that the position of the σ^* edge correlates with the bond length[14] and, therefore, a distribution of bond lengths should yield broad features in the spectra.

Figure 3 shows the B 1*s* XANES spectra for a series of BN films grown by MS and inserting HV pulses in the bias sequence. The samples are produced under different medium-energy damage values and, hence, with different levels of macroscopic stress values (see Table I), as derived from the substrate curvature method. The spectrum of the BN film with no damage (0 dpa) refers to a sample produced without HV pulses and corresponds to that shown in Fig. 2 (i.e., *c*BN with high level of stress). The samples grown below 1 dpa present a σ^* edge similar to the samples grown without HV, i.e., with a dominant fraction of sp^3 hybrids and a larger intensity at 195 eV as compared to the *c*BN reference. For damage above 1 dpa, a clear increase of the sp^2 signal at 192 eV occurs. The above results show that the microscopic structure of the *c*BN grains is stable against medium-energy ion bombardment in the low dpa range, in agreement with our previous XRD observations.[17] In addition, the appreciable transformation into *h*BN content above 1 dpa has also observed from bulk sampling methods such as Fourier transform IR spectroscopy.[9]

In the low damage range (<1 dpa), very subtle changes are observed in the B 1*s* spectra where, at the same time, a wide range of macroscopic stress values has been measured (see Table I). This can be explained due to the surface character of the XANES-TEY signal (sampling depth of 10–20 nm) and taking into account that, in the damage profile (see Ref. 19), the accumulated damage in the near surface region is much lower than the stationary bulk value. Therefore, the above observations show that, under proper conditions, stress release can be attained in *c*BN films by simultaneous ion implantation without appreciable sp^3 to sp^2 transformation. This also points out that the relaxation mechanisms should be related to sp^3 atomic rearrangements, mainly the relocation of interstitials. Recently, a model based on Monte Carlo simulations has also shown the role of collisional relocations of atoms as a path for stress relaxation in *c*BN and amorphous carbon (*a*-C) structures.[31]

A very interesting observation in Fig. 3 is the progressive convergence of the σ^* line shape toward that of polycrystalline stress-free *c*BN powder by increasing the medium-energy ion damage. Since the damage value scales with the stress release, this trend indicates that the filling of states in the 194–196 eV region is proportional to the intrinsic stress within the *c*BN network, as suggested above. It can be observed that a complete relaxation is attained for damage >1 dpa since the line shape coincides with that of the polycrystalline *c*BN powder. As evidenced in the figure, this fact occurs at the expense of an appreciable *c*BN transformation into *h*BN, although the sample still retains a dominant cubic structure. The correlation between stress and the XANES spectral line shape is further checked by DFT calculations of the PDOS.

B. Density functional theory calculations of the electronic structure

In the previous section, we have attributed the modifications in the B 1*s* line shape to the presence of intrinsic stress within the cubic network and relaxation induced by the ion bombardment, excluding the contribution from *w*BN environments. In order to verify this hypothesis, we compare here the calculated electronic structure of the *c*BN structure subjected to positive and negative stretching distortions along the {111} direction against the XANES line shape.

The PDOS projected on the B atoms for a wide range of *c* values are shown in Fig. 4. The experimental spectra from *c*BN and *h*BN reference materials are also shown to highlight the trends. The calculated PDOS have all been referenced to the top of the valence band, whereas the experimental data were shifted to align the prominent features with those in the calculations. For the two limiting cases, i.e., the *c*BN and *h*BN structures, the theoretical spectra are similar to previously reported calculations.[24,32] The increase in the PDOS at lower energies for increasing values of *c* predicts a *c*BN transformation into *h*BN upon stretching. This result is expected since, as the fourfold coordinated atoms in the sp^3 arrangement are elongated, the "buckling" of the tetrahedron decreases until it adopts an sp^2 planar configuration. This transition can be clearly appreciated in Fig. 5, where the total energy difference and static pressure are calculated as a function of the *c* value. There is a clear energy minimum (zero pressure) for the cubic phase at $c \sim 0.21$ nm, yielding a result close to the experimental value of 0.2087 nm. For larger values of *c*, a linear regime sets up at about $c=0.22$ nm, until a maximum is reached at $c=0.24$ nm, which represents the turning point toward the *h*BN structure. At this crossover, the pressure is suddenly released, implying the disappearance of any σ bonding between the BN layers.

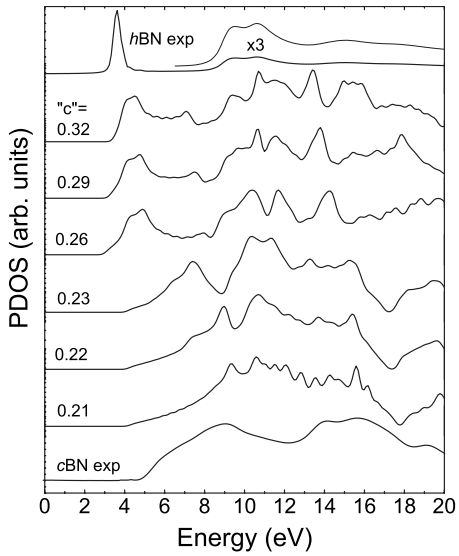

FIG. 4. DFT calculations of the PDOS for B atoms as a function of the stretching parameter c in nm. The measured spectra of polycrystalline cBN and hBN powders are shown for comparison with experimental data. The trend shows a transition from cBN to hBN under structure stretching.

Due to the elastic properties of cBN, a small mechanical perturbation in the structure leads to a large value of stress (see Fig. 5). Experimentally, XRD has shown that a variation of ~1% in the lattice parameter is responsible for the stress values in our films of ~8–10 GPa.[17] Therefore, in order to compare the calculations with our experimental results, we have focused on small perturbations of the system, i.e., c changes around the equilibrium value of ~0.21 nm. The results for this window are shown in Fig. 6. The pressure induced by these deformations is also displayed in the figure label, showing that the elongation of the structure results in negative pressure values corresponding to a compressive stress, as observed experimentally. Note that the values of pressure (up to −15 GPa) for distortions of ~5% are similar to the experimental stress levels. It is remarkable that the intensity in the PDOS for the states in the 6–8 eV region

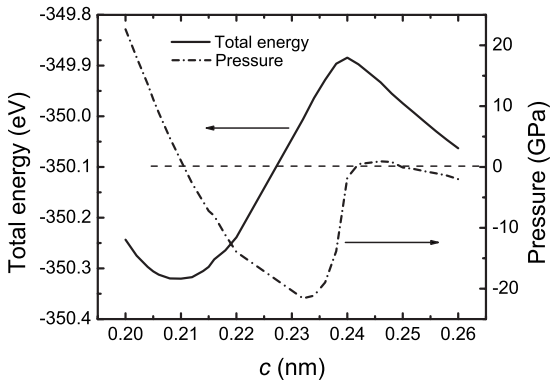

FIG. 5. Calculated (a) total energy difference and (b) static pressure for the stretched cBN structure as a function of the periodicity along the {111} direction, c.

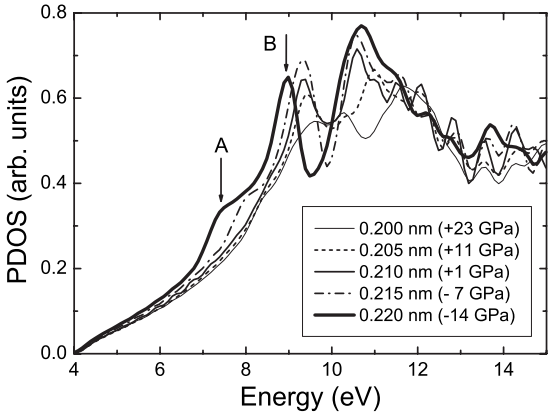

FIG. 6. DFT calculations of the PDOS for B atoms in the perturbed cBN structure along the {111} direction after imposing different pressures with values similar to experimental stress levels.

increases at negative pressure values ($c>0.21$ nm). These states are located near the onset of the unoccupied PDOS and must be related with the XANES intensity above the threshold for $1s\rightarrow\sigma^*$ transitions at 194 eV. Hence, our calculations predict the filling of states close to the σ^* onset due to the presence of stress within the cubic atomic network. This trend fits with the observed intensity increase in the 194–197 eV region (see Figs. 2 and 3). In this sense, the two dominant peaks in the low-energy region of the PDOS are labeled as A and B in correspondence with the features marked in the XANES spectra of Fig. 2. The theoretical curves predict not only the filling of state A but also the downshifting of peak B with increasing stress, in agreement with the data of Fig. 2. Based on this hypothesis, the stress relaxation induced by the medium-energy bombardment effectively reduces the strain inside cBN grains, as revealed by the convergence to the spectral line shape of the stress-free cBN sample (see Fig. 3).

V. CONCLUSIONS

In conclusion, we have studied the B 1s XANES spectra of cBN films grown by MS with different levels of intrinsic stress. The film stress was tuned by the damage induced from simultaneous medium-energy ion implantation during growth. Stress relaxation for dpa below 1 is attained while keeping the cubic structure. This finding shows that the stress release takes place at a microscopic level and originates from atomic rearrangements in the sp^3 matrix (relocation of interstitials and vacancies), without affecting the cBN grains size. Stress-free samples are produced for ion damage >1 dpa but at the expense of inducing substantial cBN transformation into hBN.

The line shape of the σ^* edge for samples with high intrinsic stress differ from the spectrum of stress-free polycrystalline cBN. The contribution from different BN phases does not yield a satisfactory fitting of the spectrum and, hence, this fact is attributed to the presence of stress and distortion within the cubic network. Hence, the broadening of the edge can be understood as a distribution of bond lengths originat-

ing from disorder, atomic mixing of different bonding environments, and bond distortion due to stress. The comparison of the XANES spectra from *c*BN samples grown with different degrees of simultaneous ion damage during growth supports the influence of stress on the spectral line shape.

The assumption that stress within the cubic network reflects in the B 1*s* line shape has been further addressed by DFT calculations of the PDOS in *c*BN structures perturbed from equilibrium under stretching. A correlation between theoretical predictions and experimental trends has been found. This fact points out the potential of XANES to detect stress in disordered BN systems.

ACKNOWLEDGMENTS

This work has been supported under DFG (Germany) Contract No. FU 303/2-2 and the Spanish Commission of Science and Technology under Contract Nos. NAN2004-09125-C07-06 and MAT2007-66719-C03-02. The synchrotron work at BESSY-II was supported by the EC "Research Infrastructure Action" under the FP6 "Structuring the European Research Area Programme" through the Integrated Infrastructure Initiative Integrating Activity on Synchroton and Free Electron Laser Science—Contract No. R II 3-CT-2004-506008.

*Author to whom correspondence should be addressed; FAX: +34 91 497 3623; raul. gago@uam.es

[1] P. Mirkarimi, K. McCarty, and D. Medlin, Mater. Sci. Eng., R. **21**, 47 (1997).
[2] W. Fukarek, J. Vac. Sci. Technol. A **19**, 2017 (2001).
[3] S. Ulrich, H. Erhardt, J. Schwan, W. Donner, H. Dosch, P. Widmayer, and P. Ziemann, Surf. Coat. Technol. **166-169**, 269 (1999).
[4] G. Reisse, S. Weissmantel, and D. Rost, Diamond Relat. Mater. **11**, 1276 (2002).
[5] J. Ullmann, A. J. Kellock, and J. E. E. Baglin, Thin Solid Films **341**, 238 (1999).
[6] C. Fitz, W. Fukarek, and W. Möller, Thin Solid Films **408**, 155 (2002).
[7] H.-G. Boyen, P. Widmayer, D. Schwertberger, N. Deyneka, and P. Ziemann, Appl. Phys. Lett. **76**, 709 (2000).
[8] C. Fitz, A. Kolitsch, W. Möller, and W. Fukarek, Appl. Phys. Lett. **80**, 55 (2002).
[9] B. Abendroth, R. Gago, A. Kolitsch, and W. Möller, Thin Solid Films **447-448**, 131 (2004).
[10] W. Donner, H. Dosch, S. Ulrich, H. Erhardt, and D. Abernathy, Appl. Phys. Lett. **73**, 777 (1998).
[11] S. Fahy, Phys. Rev. B **51**, 12873 (1995).
[12] S. Ilias, V. Stambouli, J. Pascallon, D. Bouchier, and G. Nouet, Diamond Relat. Mater. **9**, 1867 (2000).
[13] C. Fitz, W. Fukarek, and W. Möller, Diamond Relat. Mater. **11**, 1532 (2002).
[14] J. Stöhr, *NEXAFS Spectroscopy* (Springer, Berlin, 1992).
[15] A. Chaiken, L. J. Terminello, J. Wong, G. L. Doll, and C. A. Taylor II, Appl. Phys. Lett. **63**, 2112 (1993).
[16] J. C. Jan, P. D. Babu, H. M. Tsai, C. W. Pao, J. W. Chiou, S. C. Ray, K. P. Krishna Kumar, W. F. Pong, M.-H. Tsai, C. A. Jong, and T. S. Chin, Appl. Phys. Lett. **86**, 161910 (2005).
[17] B. Abendroth, R. Gago, F. Eichhorn, and W. Möller, Appl. Phys. Lett. **85**, 5905 (2004).
[18] C. Fitz, W. Fukarek, A. Kolitsch, and W. Möller, Surf. Coat. Technol. **128-129**, 474 (2000).
[19] R. Gago, M. Vinnichenko, B. Abendroth, A. Kolitsch, and W. Möller, J. Vac. Sci. Technol. A **21**, 1739 (2003).
[20] M. M. M. Bilek and D. R. McKenzie, Surf. Coat. Technol. **200**, 4345 (2006).
[21] J. J. Rehr, W. Schattke, F. J. García de Abajo, R. Díez Muiño, and M. A. Van Hove, J. Electron Spectrosc. Relat. Phenom. **126**, 67 (2002).
[22] E. L. Shirley, Phys. Rev. Lett. **80**, 794 (1998).
[23] J. J. Rehr, R. C. Albers, and S. I. Zabinsky, Phys. Rev. Lett. **69**, 3397 (1992).
[24] K. Lawniczak-Jablonska, T. Suski, I. Gorczyca, N. E. Christensen, K. E. Attenkofer, R. C. C. Perera, E. M. Gullikson, J. H. Underwood, D. L. Ederer, and Z. Liliental Weber, Phys. Rev. B **61**, 16623 (2000).
[25] N. Troullier and J. L. Martins, Phys. Rev. B **43**, 1993 (1991).
[26] J. M. Soler, E. Artacho, J. D. Gale, A. García, J. Junquera, P. Ordejdón, and D. Sánchez-Portal, J. Phys.: Condens. Matter **14**, 2745 (2002).
[27] J. P. Perdew, J. A. Chevary, S. H. Vosko, K. A. Jackson, M. R. Pederson, D. J. Singh, and C. Fiolhais, Phys. Rev. B **46**, 6671 (1992).
[28] D. M. Ceperley and B. J. Alder, Phys. Rev. Lett. **45**, 566 (1980).
[29] T. Soma, A. Sawaoka, and S. Saito, Mater. Res. Bull. **9**, 755 (1974).
[30] R. Gago, I. Jiménez, T. Sajavaara, E. Rauhala, and J. M. Albella, Diamond Relat. Mater. **10**, 1165 (2001).
[31] B. Abendroth, H. U. Jäger, W. Möller, and M. Bilek, Appl. Phys. Lett. **90**, 181910 (2007).
[32] J. B. MacNaughton, A. Moewes, R. G. Wilks, X. T. Zhou, T. K. Sham, T. Taniguchi, C. Y. Chan, W. J. Zhang, I. Bello, S. T. Lee, H. Hofsäss, and K. Watanabe, Phys. Rev. B **72**, 195113 (2005).